Applied Catalysis B: Environmental 113–114 (2012) 79–86

Contents lists available at SciVerse ScienceDirect

Applied Catalysis B: Environmental

journal homepage: www.elsevier.com/locate/apcatb

Synthesis and photocatalytic activity of Mn-doped TiO_2 nanostructured powders under UV and visible light

V.D. Binas[a], K. Sambani[a,b], T. Maggos[c], A. Katsanaki[c], G. Kiriakidis[a,b,*]

[a] Institute of Electronic Structure and Laser (IESL), FORTH, P.O. Box 1527, Vasilika Vouton, 711 10 Heraklion, Crete, Greece
[b] University of Crete, Physics Department 710 03 Heraklion, Crete, Greece
[c] Environmental Research Lab/INT-RP, NCSR "Demokritos", Agia Paraskevi Atttikis, Greece

ARTICLE INFO

Article history:
Received 9 June 2011
Received in revised form
14 November 2011
Accepted 16 November 2011
Available online 23 November 2011

Keywords:
Mn-doped TiO_2 nanoparticles
Photocatalysis under UV/visible light
Degradation of NO_x
Heterogeneous photocatalytic oxidation
In-door depollution

ABSTRACT

A straight forward, simple and inexpensive process has been developed by sol–gel method for the synthesis of manganese (Mn) doped and undoped TiO_2 photocatalysts. X-ray powder diffractometry (XRD), scanning electron microscopy (SEM) and transmission electron microscopy (TEM) revealed the presence of structural nanoparticles with an average nanocrystalline size of about 20 nm. FT-IR/vis adsorption has shown enhanced sub-band-gap absorption as a function of Mn concentration. The photocatalytic activity of these materials was evaluated by the degradation of a basic Methylene Blue (MB) as organic contaminant. Mn-doped TiO_2 powder with molar ratio 0.1:100 was mixed with calcareous filler (5% and 10% respectively) and the photocatalytic activity was evaluated by the degradation of inorganic pollutants such as NO_x under UV and visible light.

© 2011 Elsevier B.V. All rights reserved.

1. Introduction

Titanium dioxide (TiO_2) has been widely studied particularly since the discovery of its photocatalytic properties by Fujishima and Honda in 1972 [1]. Some of the current promising applications for TiO_2 nanomaterials include its content in paints [2], and toothpastes [3], while it is used also for UV protection, in photocatalysis [4,5], in photovoltaics, in gas sensing, in electrochromics as well as photochromics [6]. As a catalyst, TiO_2 nanomaterials are very stable, nontoxic, cheap and have high photocatalytic reactivity in the elimination of pollutants in air and water [7]. A very important application of TiO_2 photocatalysts is in the purification of indoor and outdoor air [8]. Malodorous substances such as ammonia, hydrogen sulfide, formaldehyde, acetaldehyde, toluene, etc., constitute potential risks to human health and comfort. Fortunately, these dangerous volatile organic compounds (VOCs) oxidize in the presence of TiO_2 nanomaterials into harmless compounds such as CO_2 and H_2O under irradiation with UV and visible light [9–22]. The catalytic mechanism is based on the excitation of electrons from the valence band (VB) to the conduction band (CB) of the TiO_2, leaving holes in the Valence Band. These electrons (e^-) and holes (h^+) can then initiate redox reactions with molecular species adsorbed on the surface of the catalyst.

Titanium dioxide can have three different crystalline phases – *rutile* (R), *anatase* (A) and *brookite* (B). There are a large number of publications reporting on the effect of phase composition and particle size on the efficiency and the photocatalytic degradation of organic pollutants. Some demonstrate that *anatase* has a higher photocatalytic activity than rutile, while in others the best performance is related to rutile [23–27]. Many experimental data indicate that mixed phases, with small amount of rutile, can facilitate the separation of photogenerated charge carriers and this enhances the photocatalytic activity [28].

Anatase TiO_2 has an energy band gap of 3.2 eV and can be activated by UV radiation with a wavelength up to 387 nm thus limiting its application as a photocatalyst under visible light illumination. However, doped with transition metal ions, the TiO_2 matrix has been frequently reported to suppressing charge carrier recombination and facilitates the onset shift in the band gap absorption to the visible region, thus enhancing its photocatalytic activity [29]. Choi et al. performed a systematic study of TiO_2 nanoparticles doped with 21 metal ions by the sol–gel method and found that the presence of metal ion dopants significantly influenced the photoreactivity, charge carrier recombination rates, and interfacial electron-transfer rates [30]. Paola et al. have investigated the doping of Co, Cr, Cu, Fe, Mo, V and W into TiO_2 matrix prepared by wet impregnation method [31]. Nagaveni et al. reported an inhibitory

* Corresponding author.
E-mail address: kiriakid@iesl.forth.gr (G. Kiriakidis).

0926-3373/$ – see front matter © 2011 Elsevier B.V. All rights reserved.
doi:10.1016/j.apcatb.2011.11.021

effect for the dopants W, V, Ce, Zr, Fe and Cu prepared by the solution combustion method [32] while few researchers have claimed the enhanced activity for these dopants compared to undoped TiO_2 in photocatalysis [33]. Kumar and co-workers have studied the photocatalytic activity of aniline blue under UV/solar light for the dopants Mn^{2+}, Ni^{2+}, and Zn^{2+} into the TiO_2 matrix [34].

In this work, we report on the synthesis and characterization of TiO_2 nanomaterials doped with manganese (Mn) in different concentrations capable to absorb and activate under visible light irradiation. The Mn-doped TiO_2 (Mn:TiO_2) powders were prepared by a modified sol–gel method. The photocatalyst was synthesized [patent GR20090100724] following a few simple synthetic steps listed below with two different precursors namely titanium (IV) tetra-isopropoxide ($Ti\{OCH(CH_3)_2\}_4$) and titanium (IV) oxysulfate ($TiOSO_4xH_2O$). Photocatalytic material may be obtained with the same physical properties, the same structure and almost the same photocatalytic activity regardless of the above precursors involved. However, the titanium (IV) tetra-isopropoxide is expensive and the synthesis requires organic solvents which increase the price of the final product; also the synthesis is harder to scale up, in contrast with the titanium (IV) oxysulfate ($TiOSO_4xH_2O$) precursor applied here. To improve the photocatalytic activities we doped TiO_2 with manganese and carried out a study of its photocatalytic activity using UV and visible light as source of radiation with Methylene Blue (MB) as the test contaminant. These photocatalytic materials may be incorporated either into concrete surfaces or applied as coatings (i.e. in walls roofs and floors) for indoor depollution applications. They may also be applied in out-door applications (i.e. sidewalks, landscaping of buildings, parking lots, etc.), contributing to improved air quality and urban environments through the reduction of pollutant agents.

In the present work, we studied the photocatalytic activity of Mn:TiO_2 powders through the degradation of a basic MB organic contaminant. Further on we mixed the above photocatalytic powders with calcareous filler base coatings. Mn:TiO_2 powders alone as well as special coatings/overlays of calcareous base with 5% and 10% powder were prepared and studies were carried out on their photocatalytic activity using UV and visible light as source of radiation towards NO_x, as inorganic pollutant.

2. Experimental

2.1. Preparation of undoped and Mn doped TiO_2

Titanium (IV) oxysulfate hydrate ($TiOSO_4{\cdot}xH_2O$), manganese (II) acetate tetrahydrate, ≥99% and titanium (IV) tetraisopropoxide [$Ti(OCH(CH_3)_2)_4$] purchased from Aldrich were applied. The Mn doped TiO_2 was prepared by a modified sol–gel method. The photocatalyst was obtained by precipitating titanium dioxide on a sol of manganese dioxide, as shown in the flowchart of the synthesis employing $TiOSO_4$ of Fig. 1. The hydrated manganese dioxide sol was obtained by mixing the required volumes of manganese acetate, i.e. $Mn(CH_3COO)_2$, 0.1 M and potassium permanganate $KMnO_4$, 0.1 M solutions and stirring the mixture for 24 h at room temperature. The obtained sol was mixed with a solution of $TiOSO_4$. The concentration of $TiOSO_4$ in the final solution was 0.1 M. The colloidal solution was stirred (Fig. 1/step1) at room temperature for 48 h, in order to obtain the adsorption equilibrium. During this phase an exchange of Mn with Ti occurs and the final sol was a mixture of both dioxides. After this step, the remaining Ti^{4+} ions were forced to precipitate by adding NH_3 solution so that the final pH was 7 (step 2). Gel so formed was stirred continuously at room temperature for aging (48 h). After aging the sol was separated using centrifuging or alternatively it was filtered under vacuum, to obtain a powder (steps 3–4). The powder was than washed (step 5) with distilled water until free of sulfate and ammonium ions. The powder was free of sulfate and ammonium ions when the test of sulfate and ammonium was negative. If the test was positive, the procedure (step 5) was repeated. The powders, after drying at 100 °C, were calcined for 3 h at 700 °C. Mn was loaded in TiO_2 with molar ratio in different concentrations between 0 and 1 wt%.

Furthermore, samples of calcareous filler containing 0%, 5% or 10% of the 0.1% Mn:TiO_2 photocatalyst were deposited on 0.25 m × 0.25 m glass panels.

2.2. Photocatalytic experiments

Photocatalytic degradation of MB ($C_{16}H_{18}ClN_3S$) in aqueous solution (10 mg L^{-1}) was carried out under UV (310–400 nm wavelength) using a mercury Lamp (Spectroline ultraviolet quartz pencil lamp/I = 4.5 mW cm^{-2}) and visible-light (Osram Dulux, 11 W) irradiation. About 100 mg of photocatalyst was added into a 100 ml of aqueous MB (10 ppm) solution. Prior to irradiation, the suspensions were sonicated in the dark for 30 min to ensure establishment of an adsorption–desorption equilibrium among the photocatalyst, MB and atmospheric oxygen. After recovering the catalyst by centrifuging, subsequent variations in the MB concentration were analyzed by an Ultraviolet–visible spectrophotometer (VARIAN Cary 50) and the adsorption peak at 664 nm (λ_{max} for MB) was recorded.

The photocatalytic activity of calcareous paint (containing 5% and 10% of the 0.1 wt% of Mn:TiO_2) was examined employing a photocatalytic system which was comprised of a gas delivery unit, a reactor chamber and a measurement unit (Fig. 2). A compressed gas cylinder of 10 ppmv NO (±2%) balanced in N_2 was used for the creation of NO_x polluted atmosphere in the photocatalytic reactor (Linde Hellas Ltd.). Prior to its introduction to the photocatalytic chamber, NO was mixed with the appropriate quantity of synthetic air (20.5% v/v O_2 and 79.5% v/v N_2) adjusting the initial NO_x concentration to C_{NO} = 250 μg m^{-3}.

Photocatalytic experiments were carried out in a cubic pyrex glass reaction chamber of 0.125 m^3 volume capacity (50 cm × 50 cm × 50 cm) which was placed inside a (light) sealed irradiation box. The photocatalytic films were placed at the bottom surface of the cell. The cell's loading factor l_f (photocatalyst surface/cell volume ratio) was estimated to be about 0.442 m^2 m^{-3}.

Illumination was provided by ten 15 W Philips TLD 15 W/08 fluorescent black light blue type, or ten vis lamps (PHILIPS $FSL_{YZ15RR26}$) being placed horizontally in pairs on each side of the irradiation box at a distance of approximately ~20 cm from the photocatalytic material. The total light intensity measured on the samples' surface by the ten TLD lamps was on average 2.6 W m^{-2}, of which 55% (1.43 W m^{-2}) was due to UV. The corresponding total light intensity value for the 10 FSL lamps (vis) was 7.6 W m^{-2}, of which only the 0.6% was attributed to UV. The irradiation time was set in 45 min. The environmental box was also further equipped with two fans for keeping the temperature stable.

The initial concentration of the air pollutant as well as the adopted temperature and humidity levels into the inner environment of (inside) the glass cell were chosen with the ultimate criterion of approaching the corresponding levels of the same variables in the outdoor real environment. For that purpose the NO concentration was established at approximately 250 μg m^{-3}, while the temperature and humidity levels were controlled at 24–27 °C and 35–45% respectively. The NO_x concentration was measured with a chemiluminescence NO_x analyzer (Environment S.A AC42M) which was connected in line to the outlet of the reactor.

2.3. Characterization of manganese-doped TiO_2 nanoparticles

The crystal structure, particle size, morphology, and porosity were examined with an XRD-powder system, SEM, TEM and

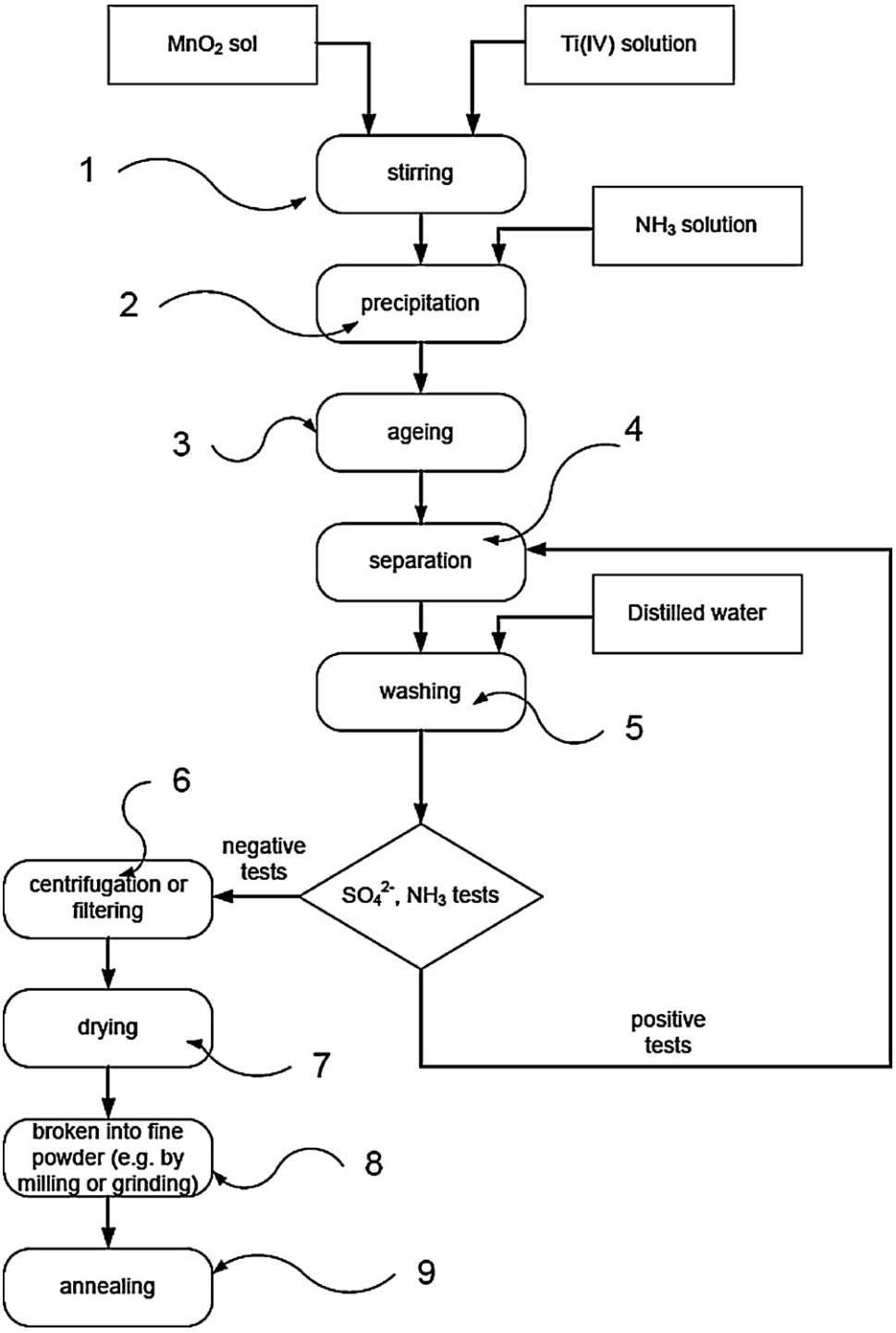

Fig. 1. Synthetic procedure of Mn:TiO_2.

porosimetry respectfully. Powder X-ray diffraction patterns were obtained on a Rigaku D/MAX-2000H rotating anode diffractometer (CuKα radiation) equipped with the secondary pyrolitic graphite monochromator operated at 40 kV and 80 mA over the 2θ collection range of 20–80°. The scan rate was $0.02^\circ\ s^{-1}$. N_2 sorption isotherms were recorded on a commercial volumetric system (Autosorb 1-MP, Quantachrome). Typically, 100 mg of sample was used to record adsorption isotherms. Surface morphology and elemental analysis of the samples were carried out using scanning electron microscopy (SEM) and an energy dispersive spectrometer (EDS) on a JSM-6390LV instrument. The microscopic nanostructures were observed by TEM on a JEM-2100 instrument equipped with LaB_6 filament, operating at 200 kV.

3. Result and discussion

3.1. Structural and optical properties of nanoparticles manganese-doped TiO_2 nanoparticles

The XRD patterns of composite nanostructured powders with different concentrations (0, 0.1, 0.5 and 1 wt%) of Mn:TiO_2 calcined at 700 °C are shown in Fig. 3. For all samples, the anatase phase was

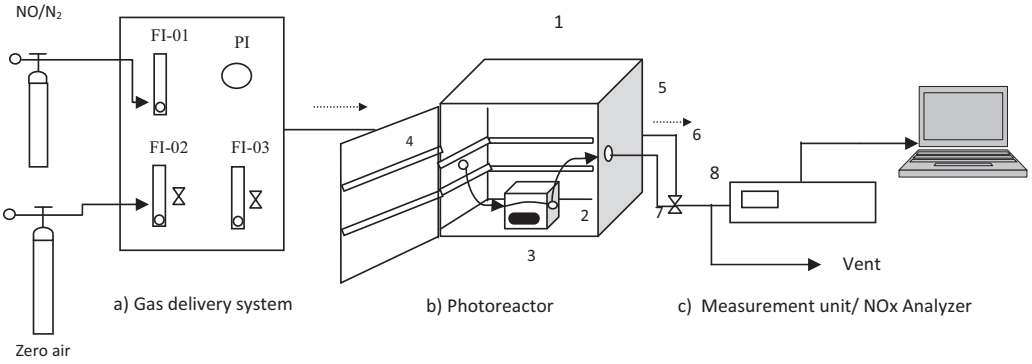

Fig. 2. Schematic presentation of the photocatalytic apparatus where FI: flow controller/indicator; PI: pressure indicator; 1: irradiation box; 2: reaction chamber (0.125 m^3); 3: Mn:TiO_2 sample (0.05525 m^2); 4: UV–vis or UV Lamps (10); 5: fans (2); 6: by-pass line; 7: base line; 8: sampling line.

detected with corresponding values at $2\theta = 25.3^\circ$ for plane (1 0 1), 38° for (0 0 4), and 48° for (2 0 0). The grain size (D) for all samples was in the range of 20–30 nm and it was determined from the full width at half maximum (FWHM) of the (1 0 1) anatase peak according to the Scherrer's formula, $D = k\lambda/w\cos\theta$ [where k is the shape factor (~0.9), λ the X-ray wavelength (0.15418 nm), and θ the diffraction angle].

Fig. 4 shows the effect of calcination temperature on the structure of the XRD patterns of 0.1% Mn:TiO_2. A monotonic increase of the intensity of the peaks in the temperature range of 200–700 °C was obtained. All samples in the above range of calcination temperatures were monophasic with only the anatase polymorph TiO_2 been detected.

The BET (Brunauer–Emmet–Teller) surface area of the Mn:TiO_2 composites with different concentration of Mn (0.1%, 0.5% and 1%) calcined at 700 °C for 3 h was calculated at 24, 30 and 38 $m^2\,g^{-1}$, respectively.

Absorption studies on the said material as a function of Mn concentration presented in a recent publication of Papadimitriou et al. [35] elaborate on the role of Mn in the induced catalytic behavior of 0.1% Mn:TiO_2. It was found that at an optimum dopant concentration of 0.1% the material absorption is maximum, an observation that is in line with past reports by Ullah and Dutta [36] on a Mn doped ZnO system. It is believed that at very low concentrations (<0.5%) Mn, taking interstitial or substitutional sites in TiO_2 matrix, is contributing to the enhancement of the material absorption with a corresponding red-shift. At higher concentrations significant structural changes of TiO_2 may take place with manganese, in the form of Mn^{2+}, reacting preferably with oxygen to form MnO_x. Thus, we observed a reduction in the optical absorption with further increase in the dopant concentration and the existence of an optimum at 0.1% Mn doping.

The textural features of the samples were investigated with scanning electron microscopy. Representative images of composites in different concentrations for 0%, 0.1%, 0.5% and 1% Mn:TiO_2 are shown on Fig. 5 demonstrating no specific morphology changes apart of a trend for surface particle agglomeration. Corresponding energy dispersive X-ray spectroscopy (EDX) indicated the presence of Mn and TiO_2 nanocomposites. TEM images of the 1% Mn:TiO_2 composite confirmed the agglomeration of particles with size estimated about 20–30 nm (Fig. 6).

3.2. Photocatalytic properties

3.2.1. Degradation of Methylene Blue (MB)

The photocatalytic activities of undoped and Mn:TiO_2 were carried out using UV light and visible light. MB was used as the test contaminant, a dye extensively used as an indicator for the study of photocatalytic activities [37,38] exhibiting absorption peak (s) in the visible range. Thus, degradation can be easily monitored by optical absorption spectroscopy analyzing the evolution of the 675 nm MB peak. The recorded decolarization of MB under UV and vis light in the absence of photocatalytic material (shown in Figs. 7 and 8) might be due to the interaction of MB with $OH^\bullet$

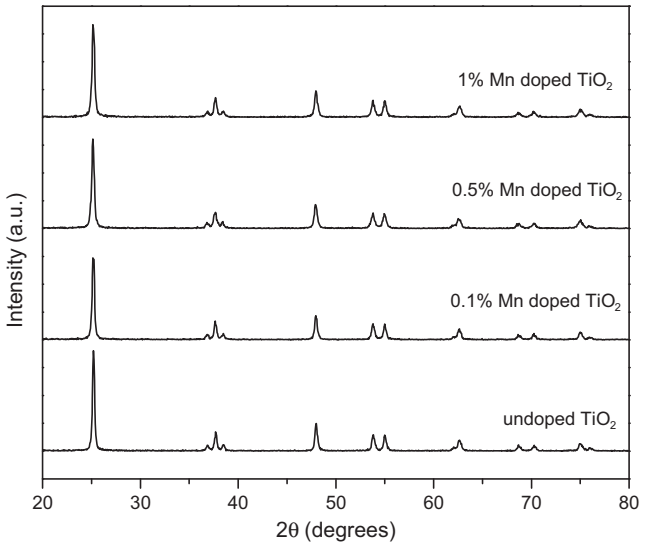

Fig. 3. Powder XRD patterns of undoped and Mn doped TiO_2 samples in different concentration of manganese.

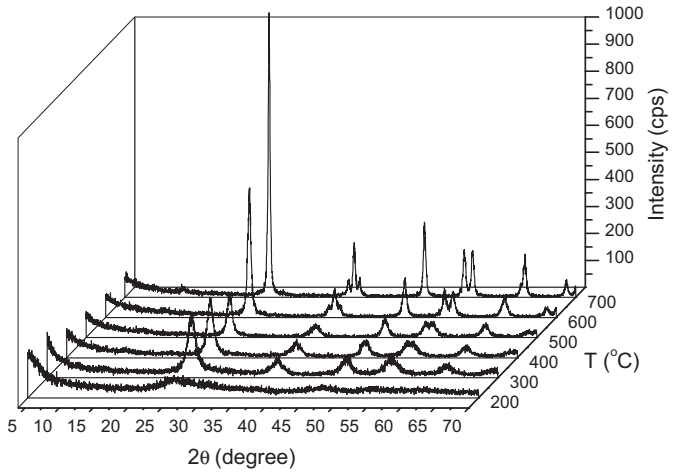

Fig. 4. Powder XRD patterns in different calcinations temperatures of 0.1% Mn:TiO_2.

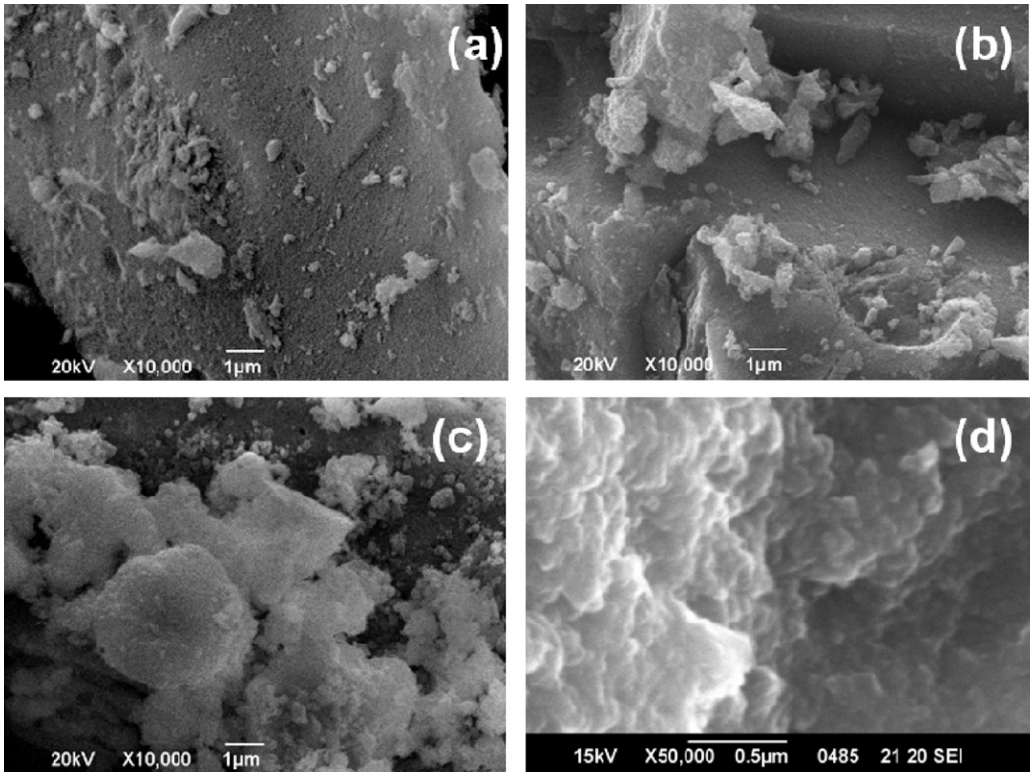

Fig. 5. Scanning electron microscopy (SEM) images of Mn:TiO_2 powders in different concentrations (a: undoped TiO_2, b: 0.1%, c: 0.5%, d: 1%).

radicals originated from water [39]. In our tests we first studied the photodegradation of MB in pure TiO_2 and subsequently in Mn:TiO_2 in different loadings (0.1%, 0.5%, 1%) by irradiating a mixture of photocatalyst and MB with UV light. It was observed that doped TiO_2 decolorizes MB in a monotonic way with a decolorization decreasing as increasing the loading of Mn doping. Superior decomposition efficiency for the 0.1% Mn material with respect of all other compositions was recorded. However in all tests under UV light we did not record any significant improvement on decolorization efficiencies between the 0.1% Mn doped and the undoped TiO_2 materials (Fig. 7). In contrast with the above, the photo-degradation rate of MB with 0.1% Mn:TiO_2 irradiated with visible light was found to be faster than with other loadings as well as that of the undoped TiO_2 as shown in Fig. 8. It was recorded that it only takes 20 min for 0.1% Mn:TiO_2 to decolorize as much as 70% of MB while in the presence of undoped TiO_2 the decolorization was only 40% for the same time scale (Figs. 9 and 10).

3.2.2. *Degradation of NO_x*

The photocatalytic removal of NO from 0.1% of Mn:TiO_2 powder in calcareous matrices containing 5% and 10% of the photocatalytic material was evaluated under both UV and vis irradiation. Photocatalytic experiments were conducted in order to distinguish the pure UV or vis photocatalytic effect of the TiO_2 powders from the NO_x reduction due to its adsorption on the cell walls and/or its radiation photolysis. Thus, initially, blank tests were carried out by polluting the reactor with NO in the absence of the photocatalyst without

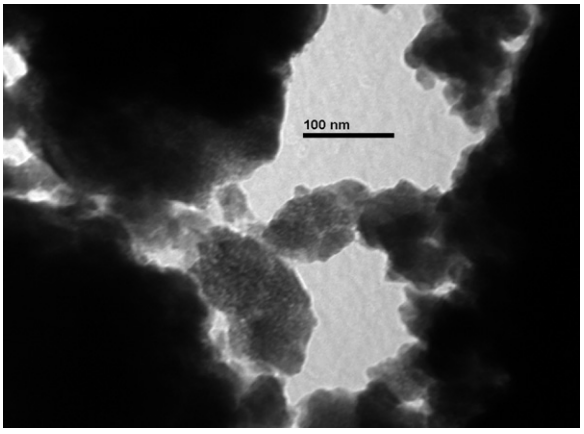

Fig. 6. TEM image of the Mn:TiO_2 (1:100).

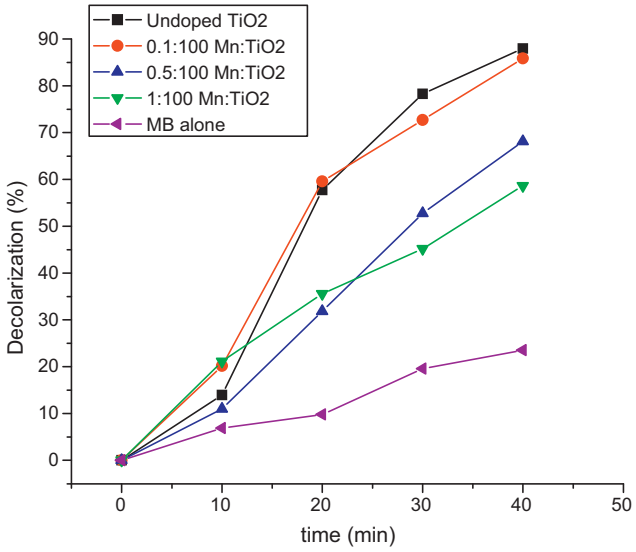

Fig. 7. Degradation of Methylene Blue (MB) under UV light.

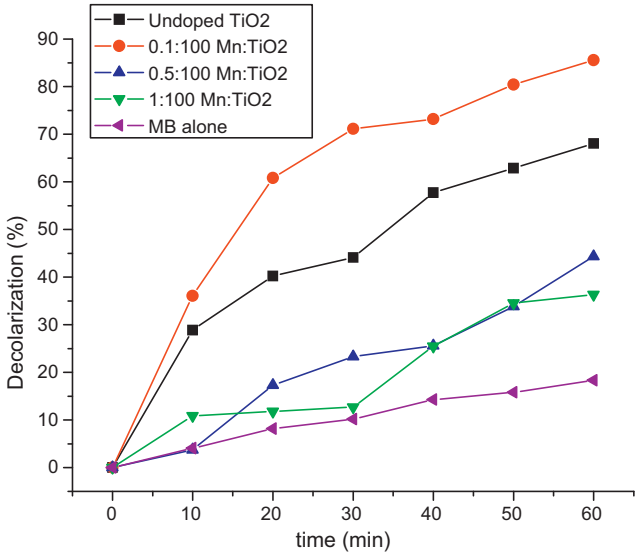

Fig. 8. Degradation of Methylene Blue under visible light.

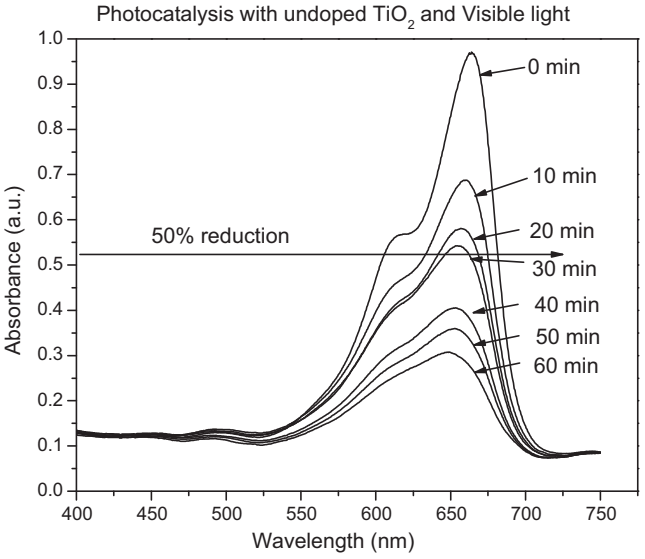

Fig. 9. Photo-reduction of MB with undoped TiO_2 and visible light.

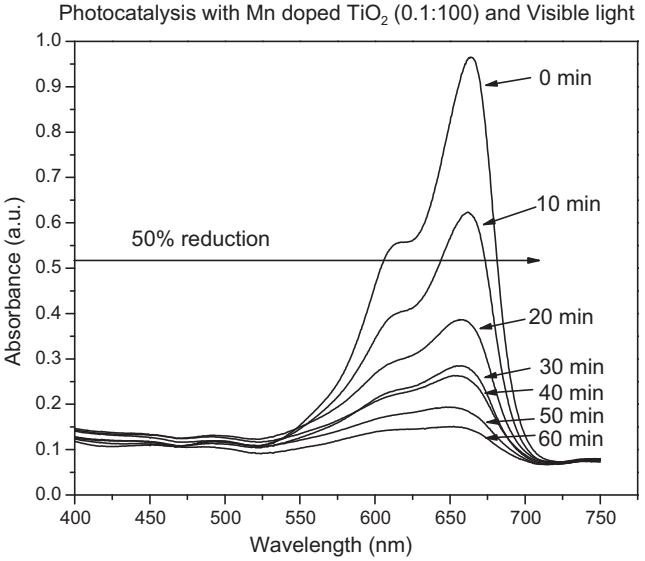

Fig. 10. Photo-reduction of MB with Mn:TiO_2 and visible light.

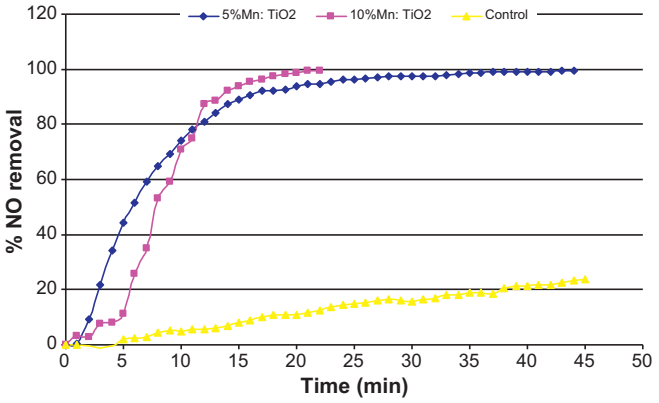

Fig. 11. %NO degradation under UV illumination.

and with irradiation respectively. Then the same experiments were carried out in the presence of the photocatalysts.

Photodegradation graphs of the different samples under UV and vis irradiation are shown in Fig. 11 and Fig. 12 respectively. As it can be seen from both figures, immediately after the irradiation of the sample (Time 0), a significant decrease in the NO concentration is observed which reveals the immediate response of the photocatalytic system and gives the size of the photocatalytic performance of the materials. A slightly better photocatalytic ability was monitored by the 10% Mn:TiO_2 powder under both UV and vis with respect to the 5%. Additionally, it is shown (Fig. 11) that the 10% sample removes more than 99% of NO from the system after 25 min while the 5% needs more than 40 min to remove the same amount. Independent studies on the same materials and concentrations carried out by the JRC at ISPRA [40] have shown identical photocatalytic activities, thus, underlining the effectiveness of these Mn:TiO_2 powders for in-door depollution application utilizing artificial lighting.

The reduction of NO during blank tests (substrate and filler without (w/o) TiO_2) is attributed to competitive depletion mechanisms such as adsorption of NO onto the chamber's wall area and to photolysis. Calculations have shown that both these mechanisms did not contribute to more than 32% of the total NO removal during the photocatalytic experiments (Tables 1 and 2).

The above results have been further analyzed in order to quantify the photocatalytic *performance* of the TiO_2 materials under *UV or vis irradiation*. The performance of the materials was evaluated via the calculation of the following parameters: (a) the percentage

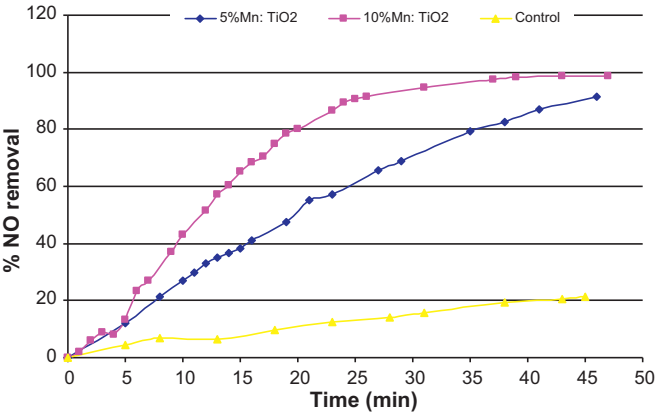

Fig. 12. %NO degradation under vis illumination.

Table 1
Material's photocatalytic activity results under UV irradiation.

Material	% NO removal	% NO photocatalytic destruction (PPD)	Photocatalytic destruction rate (DR) NO ($\mu g\,m^{-2}\,s^{-1}$)
Substrate	32 (Removal due to UV photolysis and sink effects on reactor's wall)	–	–
Calcareous filler w/o Mn:TiO_2	35	–	–
Calcareous filler with 5% Mn:TiO_2	99.5	67.5	0.151
Calcareous filler with 10% Mn:TiO_2	99.7	67.7	0.185

Table 2
Material's photocatalytic activity results under vis irradiation.

Material	% NO removal	% NO photocatalytic destruction (PPD)	Photocatalytic destruction rate (DR) NO ($\mu g\,m^{-2}\,s^{-1}$)
Substrate	30 (Removal due to vis photolysis and sink effects on reactor's wall)	–	–
Calcareous filler w/o Mn:TiO_2	30.9	–	–
Calcareous filler with 5% Mn:TiO_2	92.4	62.4	0.129
Calcareous filler with 10% Mn:TiO_2	98.8	68.8	0.130

photocatalytic degradation (PPD) and (b) the destruction rate (DR) according to the following Eqs. (1)–(2).

$$\mathrm{PPD}\,(\%) = \left[\frac{C_{in} - C_{fin}}{C_{in}}\right] \times 100 \quad (1)$$

$$\mathrm{DR}\,(\mu g/m^2 s) = (C_{in} - C_{fin}) \times \frac{V}{A \times t} \quad (2)$$

where, C_{in}, C_{fin} the initial and final NO concentrations, A the sample area and V the volume of the reactor.

The destruction rate (DR) of NO (Tables 1 and 2) provides a more accurate measure of the photocatalytic activity of the material in comparison with the photocatalytic decomposition parameter PPD (%) owing to the fact that the DR is taking into consideration the initial concentration of the air pollutant as well as the sample's area and the irradiation time and is expressed as μg of converted NO per m^2 of material per second of irradiation. As far as the 5% and 10% Mn:TiO_2 materials under UV irradiation are concerned the DR have been calculated to be 0.151 and 0.185 respectively. The corresponding experiments under vis irradiation presented slightly lower values calculated to be 0.129 and 0.130 respectively.

Currently, research is focusing on the improvement of the above synthetic procedure which, combined with further characterization of the composites nanostructure and the use of other dopand (transition metal or non metal) materials, form an extensive study on the degradation mechanism of additional volatile organic compounds (formaldehyde, toluene, benzene) and inorganic compounds (NO_x and CO) under UV and visible light for out-door and in-door applications.

4. Conclusions

Nanocrystalline Mn:TiO_2 powder of crystallite size of 20–30 nm can be synthesized by a straight forward and inexpensive procedure. The starting chemicals applied for this process are easily accessible, and are cheaper than alternative organic precursors leading to the same metal oxides powders. Anatase was found to be the major phase in all samples. FT-IR/vis adsorption has shown enhanced sub-band-gap absorption as a function of Mn concentration. The photocatalytic activity on the MB degradation of 0.1% Mn:TiO_2 was higher than the other photocatalytic material with different concentrations (0.5% and 1%) both under UV and visible light. Corresponding tests on the NO removal by calcareous bases containing 5% and 10% of the 0.1% Mn:TiO_2 powder material have shown a 99% reduction rate under UV and vis light exposure in 25 and 45 min respectfully. Corresponding maximum reduction rates were 0.185 and 0.130 (for the 10% content in the calcareous base) of the 0.1% Mn:TiO_2 powder.

Acknowledgment

Funding through the E.C. FP7 "Clear–Up" N° 211948 is acknowledged.

References

[1] K. Honda, A. Fujishima, Nature 238 (1972) 37.
[2] J.H. Braun, A. Baidins, R.E. Marganski, Prog. Org. Coat. 20 (1992) 105.
[3] S.A. Yuan, W.H. Chen, S.S. Hu, Mater. Sci. Eng., C 25 (2005) 479.
[4] M.R. Hoffmann, S.T. Martin, W. Choi, D.W. Bahnemann, Chem. Rev. 95 (1995) 69.
[5] M. Gratzel, Nature 414 (2001) 338.
[6] D.K. Hwang, J.H. Moon, Y.G. Shul, K.T. Jung, D.H. Kim, D.W. Lee, J. Sol-Gel Sci. Technol. 26 (2003) 783.
[7] L.P. Childs, D.F. Ollis, J. Catal. 66 (1980) 383.
[8] Z. Huang, P.C. Maness, D.M. Blake, E.J. Wolfrum, S.L. Smolinski, W.A. Jacoby, J. Photochem. Photobiol. A 130 (2000) 163–170.
[9] A.L. Pruden, D.F. Ollis, J. Catal. 82 (1983) 404.
[10] I. Ait-Ichou, M. Formenti, B. Pommier, S.J. Teichner, J. Catal. 91 (1985) 193.
[11] S.A. Larson, J.A. Widegren, J.L. Falconer, J. Catal. 157 (1995) 611.
[12] J.L. Falconer, K.A. Magrini-Bair, J. Catal. 179 (1998) 171.
[13] M.D. Driessen, V.H. Grassian, J. Phys. Chem. B 102 (1998) 1418.
[14] D. Brinkley, T. Engel, J. Phys. Chem. B 104 (2000) 9836.
[15] M.C. Blount, J.L. Falconer, J. Catal. 200 (2001) 21.
[16] T. Tatsuma, S. Tachibana, A. Fujishima, J. Phys. Chem. B 105 (2001) 6987.
[17] D.F. Ollis, H. Al-Ekabi (Eds.), Photocatalytic Purification and Treatment of Water and Air, Elsevier, Amsterdam, 1993.
[18] N. Serpone, E. Pelizzetti (Eds.), Photocatalysis – Fundamentals and Applications, Wiley, New York, 1989.
[19] P.D. Cozzoli, R. Comparelli, E. Fanizza, M.L. Curri, A. Agostiano, Mater. Sci. Eng., C 23 (2003) 707.
[20] S.Y. Chae, M.K. Park, S.K. Lee, T.Y. Kim, S.K. Kim, W.I. Lee, Chem. Mater. 15 (2003) 3326.
[21] Y. Bessekhouad, D. Robert, J.V. Weber, N. Chaoui, J. Photochem. Photobiol. A 167 (2004) 49.
[22] A.L. Linsebigler, G.Q. Lu, J.T. Yates, Chem. Rev. 95 (1995) 735.
[23] S.S. Watson, D. Beydoun, J.A. Scott, R. Amal, Chem. Eng. J. 95 (2003) 213.
[24] S.K. Lee, P.K.J. Robertson, A. Mills, D. McStay, N. Elliott, D. McPhail, Appl. Catal., B: Environ. 44 (2003) 173.
[25] A. Sclafani, J.M. Herrmann, J. Phys. Chem. 100 (1996) 13655.
[26] M.H. Habibi, H. Vosooghian, J. Photochem. Photobiol. A 174 (2005) 45.
[27] R. Gomez, J. Mater. Res. 10 (1995) 2788.
[28] S.T. Martin, C.L. Morrison, M.R. Hoffmann, J. Phys. Chem. 98 (1994) 13695.
[29] S. Kim, S.J. Hwang, W. Choi, J. Phys. Chem. B 109 (2005) 24260.
[30] W. Choi, A. Termin, M.R. Hoffmann, J. Phys. Chem. 98 (1994) 13669.
[31] A.D. Paola, G. Marci, L. Palmisano, M. Schiavello, K. Uosaki, S. Ikeda, B. Ohtani, J. Phys. Chem. B 106 (2002) 637.

[32] K. Nagaveni, M.S. Hegde, G. Madras, J. Phys. Chem. B 108 (2004) 20204.
[33] K.E. Karakitsou, X.E. Verykios, J. Phys. Chem. 97 (1993) 1184.
[34] L. Devi, N. Kottam, B. Murthy, S. Kumar, J. Mol. Catal. A 328 (2010) 44–52.
[35] V.C. Papadimitriou, V.G. Stefanopoulos, M.N. Romanias, P. Papagiannakopous, K. Sambani, V. Tudose, G. Kiriakidis, Thin Solid Films (2011), doi:10.1016/j.tsf.2011.07.073, http://dx.doi.org/10.1016/j.tsf.2011.07.073.
[36] R. Ullah, J. Dutta, J. Hazard. Mater. 156 (2008) 194–200.
[37] R. Wang, J.H. Xin, J. Hu, Appl. Surf. Sci. 227 (2004) 312–317.
[38] H. Lachheb, J.M. Hermman, Appl. Catal. B: Environ. 31 (2001) 145.
[39] G. Cerisola, Sep. Purif. Technol. 54 (2007) 382.
[40] C. Cacho, O. Geiss, J. Barrero-Moreno, V.D. Binas, G. Kiriakidis, L. Botalico, D. Kotzias, J. Photochem. Photobiol. A 222 (2011) 304–306.